Journal of Quantitative Spectroscopy & Radiative Transfer 302 (2023) 108587

Contents lists available at ScienceDirect

Journal of Quantitative Spectroscopy & Radiative Transfer

journal homepage: www.elsevier.com/locate/jqsrt

Ultraviolet spectroscopy of AlO from first principle

Tianrui Bai[a,b], Zhi Qin[b,c,*], Linhua Liu[b,c,d,*]

[a] School of Energy and Power, Jiangsu University of Science and Technology, Zhenjiang, Jiangsu 212100, China
[b] Optics and Thermal Radiation Research Center, Institute of Frontier and Interdisciplinary Science, Shandong University, Qingdao, Shandong 266237, China
[c] School of Energy and Power Engineering, Shandong University, Jinan, Shandong 250061, China
[d] School of Energy Science and Engineering, Harbin Institute of Technology, Harbin, Heilongjiang 150001, China

ARTICLE INFO

Article history:
Received 9 November 2022
Revised 18 February 2023
Accepted 17 March 2023
Available online 20 March 2023

Keywords:
Partition functions
Radiative lifetimes
Line intensities
Ultraviolet spectrum
AlO

ABSTRACT

The spectrum of AlO is widely used in various applications including the explorations of interstellar space, studies of laser ablation, combustions of Al-containing fuels and so on. In this work, we reported the spectroscopy of the AlO radical at temperatures of 300 ~ 15,000 K for the wavenumber range of 1 ~ 55,000 cm^{-1}. Firstly, we extended our previous calculations of the potential energy curves (PECs) and transition dipole moments (TDMs) for AlO (Bai, Qin & Liu, MNRAS, 2022, 510:1649–1656) to higher $B^2\Sigma^+$, $D^2\Sigma^+$, $1'^2\Pi$ and $1''^2\Pi$ electronic states, with the consideration of Davidson correction, scalar relativistic correction and core-valence correlation. Partition functions, Einstein coefficients and radiative lifetimes of AlO were then obtained by solving the nuclear-motion Schrödinger equation. The partition functions reveal that the AlO molecules mainly exist in the $X^2\Sigma^+$ state at temperatures of 10 ~ 6270 K and in the $A^2\Pi$ state at temperatures of 6270 ~ 15,000 K in the thermodynamic equilibrium. Finally, line intensities and spectra for different electronic transitions of AlO were calculated. The results show that the $X^2\Sigma^+ \rightarrow C^2\Pi$ and $X^2\Sigma^+ \rightarrow D^2\Sigma^+$ transitions dominate in the ultraviolet waveband. Comparisons of the TDMs, radiative lifetimes, line intensities and spectra with previous theoretical and experimental values indicate that our calculated data in the ultraviolet waveband are reliable and may be used for the radiation field calculation.

1. Introduction

The spectroscopy of aluminium monoxide (AlO) is essential for astronomical observations, since its emission lines have been detected around red supergiant VY Canis Majoris [1], oxygen-rich stars [2,3], Sunspots [4], R Aquarii [5], and so on [6–11]. Moreover, Al is the second most abundant metal in the Earth's crust and often used as a rocket fuel, as a result, considerable amounts of aluminum oxide are introduced into the atmosphere [12–15]. Reliably analyzing the detected spectra requires wide knowledge of accurate spectral lines, mostly relying on experimental observations and theoretical calculations. Hence, the study of the AlO spectrum is of crucial importance to understand the astrophysical environments or atmospheric phenomenon.

The spectrum for the blue-green ($B^2\Sigma^+$-$X^2\Sigma^+$) band system of AlO was reported experimentally by Pomeroy [16] for the first time. Since then, a series of studies on the measured spectrum of AlO have been carried out. Several electronic states of AlO, including the $X^2\Sigma^+$, $A^2\Pi$, $B^2\Sigma^+$, $C^2\Pi$, $D^2\Sigma^+$, $E^2\Delta$ and $F^2\Sigma^+$ states, and the associated electronic transitions, including the $A^2\Pi$-$X^2\Sigma^+$ [17,18], $B^2\Sigma^+$-$X^2\Sigma^+$ [18–22], $C^2\Pi$-$X^2\Sigma^+$ [18,23], $C^2\Pi$-$A^2\Pi$ [24], $B^2\Sigma^+$-$A^2\Pi$ [25] systems, have been identified experimentally in the past few decades. Molecular parameters of these electronic states have been collected by Herzberg and Huber [26]. Recently, a comprehensive overview of the experimental spectroscopy for the AlO radical was given by Bowesman et al. [27], which concluded that the $B^2\Sigma^+$-$X^2\Sigma^+$ and $A^2\Pi$-$X^2\Sigma^+$ systems were extensively studied in the experiments. However, due to a series of the limitation of experimental conditions, such as the equipment, resolution, contamination, etc., experimental data are often limited in the temperature applicability and spectral range.

Several theoretical studies for AlO have also been performed [28–37]. However, most of these studies have focused on the transition properties and spectra of the $A^2\Pi$-$X^2\Sigma^+$ and $B^2\Sigma^+$-$X^2\Sigma^+$ transitions in the infrared and visible wavebands. For example, Yoshimine et al. [29] presented the band strengths for five transitions ($X^2\Sigma^+$-$X^2\Sigma^+$, $A^2\Pi$-$A^2\Pi$, $X^2\Sigma^+$-$A^2\Pi$, $B^2\Sigma^+$- $B^2\Sigma^+$, $B^2\Sigma^+$-$X^2\Sigma^+$), but only obtained a few bands for the low vibrational levels. The ExoMol's group [27,38] used experimentally-refined potential energy and various coupling curves to calculate the line lists for the $B^2\Sigma^+$ - $X^2\Sigma^+$, $A^2\Pi$ - $X^2\Sigma^+$ and $X^2\Sigma^+$-$X^2\Sigma^+$ transitions

* Corresponding authors at: Optics and Thermal Radiation Research Center, Institute of Frontier and Interdisciplinary Science, Shandong University, Qingdao, Shandong 266237, China.
E-mail addresses: z.qin@sdu.edu.cn (Z. Qin), liulinhua@sdu.edu.cn (L. Liu).

https://doi.org/10.1016/j.jqsrt.2023.108587
0022-4073/

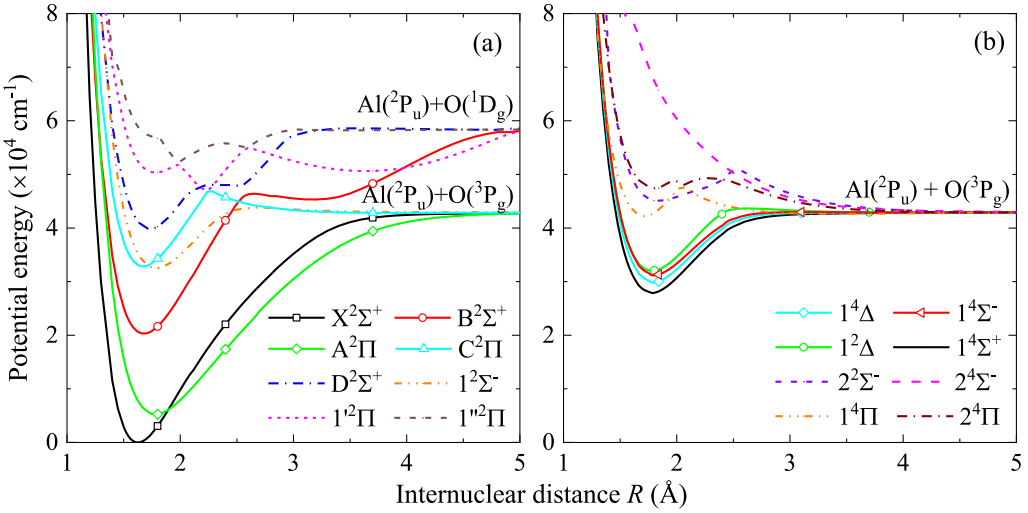

Fig. 1. Potential energy curves of sixteen electronic states for AlO. PECs of the $B^2\Sigma^+$, $D^2\Sigma^+$, $1'^2\Pi$ and $1''^2\Pi$ are calculated in this work. The other PECs are taken from our previous work [49].

of AlO, covering the wavenumbers of about 100–28,000 cm^{-1}. To obtain the spectrum in the ultraviolet waveband, Feng and Zhu [39] reported the radiative lifetimes of high electronic states ($A^2\Pi$, $G^2\Delta$, $G'^2\Sigma^-$, $B^2\Sigma^+$, $C^2\Pi$ and $D^2\Sigma^+$) of AlO, but their results were significantly different from the experimental values. Also, the ultraviolet cross sections of AlO have been not much known yet. Thus, we plan to carry out a more accurate and comprehensive theoretical investigation on a broad range of transitions in the ultraviolet waveband of AlO.

Currently, there is a lack of transition spectra for high electronic states of AlO in the ultraviolet waveband. The aim of this work is to perform a comprehensive investigation of the electronic transition properties of AlO, particularly for dipole-allowed transitions in the ultraviolet waveband. The obtained spectra are expected to provide guidelines in experimental observations and astronomical detections of AlO. Section 2 presents the state-of-art *ab initio* methods. Potential energy curves (PECs) and transition dipole moments (TDMs) are given in Section 3, together with the radiative lifetimes, line intensities and cross sections of dipole-allowed transition systems. In Section 4, conclusions are drawn.

2. Methods

2.1. Potential energy curves and transition dipole moments

In this paper, the PECs and TDMs of AlO were calculated using the internally contracted multireference configuration-interaction (icMRCI) method [40]. To consider the Davidson correction, core-valence correlation [41] and scalar relativistic correction [42], the augmented correlation-consistent polarized weighted core-valence quintuple-zeta basis set, aug-cc-pwCV5Z-DK, was chosen [43]. These calculations were carried out by the MOLPRO 2015 program package [44].

In the calculations, 12 inner electrons in the 1*s* and 2*s*2*p* shell of Al and 1*s* shell of O were put into six closed-shell molecular orbitals (MOs) in the symmetry representations of C_{2v}: four a_1 orbitals, one b_1 orbital, one b_2 orbital, and no a_2 orbitals. The remaining 9 electrons were put into 8 outermost MOs including the 3*s*3*p* shell of Al and 2*s*2*p* shell of O, which constituted the active space and was used to investigate the states correlating to the first dissociation limit. For better relaxation of the wave functions of higher electronic states, we added four MOs (3*s*3*p* shell of O) to the active space to calculate the electronic states correlating to the second dissociation limit. The orbital set was called (10, 4, 4, 0).

2.2. Radiative lifetimes

The radiative lifetime $\tau_{\upsilon'}$ of a certain vibrational level υ' for the upper electronic state can be determined by [45]

$$\tau_{\upsilon'} = \frac{1}{\sum_{\upsilon''=0}^{\upsilon''_{\max}} A_{\upsilon'\upsilon''}} \tag{1}$$

where $A_{\upsilon'\upsilon''}$ is the Einstein coefficient of the spontaneous emission from the initial (upper) electronic state i with quantum numbers Λ', υ', l' to the final (lower) state f with quantum numbers Λ'', υ'', l'' and can be calculated by [45]

$$A_{\upsilon'\upsilon''} = 2.026\times10^{-6}\nu_{if}^3\frac{2-\delta_{0,\Lambda'+\Lambda''}}{2-\delta_{0,\Lambda'}}\left[\int_0^\infty \psi_{\upsilon'}(r)R_e(r)\psi_{\upsilon''}(r)\right]^2 \tag{2}$$

where ν_{if} is the transition wavenumber, $R_e(r)$ is the TDM function, $\psi_{\upsilon'}(r)$ and $\psi_{\upsilon''}(r)$ are the vibrational wave functions of the initial and final electronic states, respectively.

2.3. Intensities and cross sections

In thermodynamic equilibrium conditions, the energy level distribution within a single molecule is assumed to follow the Boltzmann distribution, the absorption line intensity I (cm molecule^{-1}) of a single diatomic molecule can be expressed as [46]

$$I(f\leftarrow i) = \frac{g_f^{tot}A_{fi}}{8\pi c\nu_{fi}^2}\frac{\exp\left(-\frac{hcE_i}{k_BT}\right)\times\left(1-\exp\left(-\frac{hc\nu_{fi}}{k_BT}\right)\right)}{Q(T)} \tag{3}$$

where h, k_B and c are the Planck's constant, Boltzmann constant and the speed of light in vacuum, respectively. $g_f^{tot}$is the total degeneracy. E_i is the energy of the electronic state of the initial electronic state. $Q(T)$ is the partition function and can be calculated by [47]

$$Q(T) = \sum_n^{n_{\max}}(2-\delta_{\Lambda,0})(2S+1)\sum_{\upsilon}^{\upsilon_{\max}(n)}\sum_{l}^{l_{\max}(n)}(2l+1)\exp\left(-hc\frac{E_{n,\upsilon,l}-\varepsilon_0}{k_BT}\right) \tag{4}$$

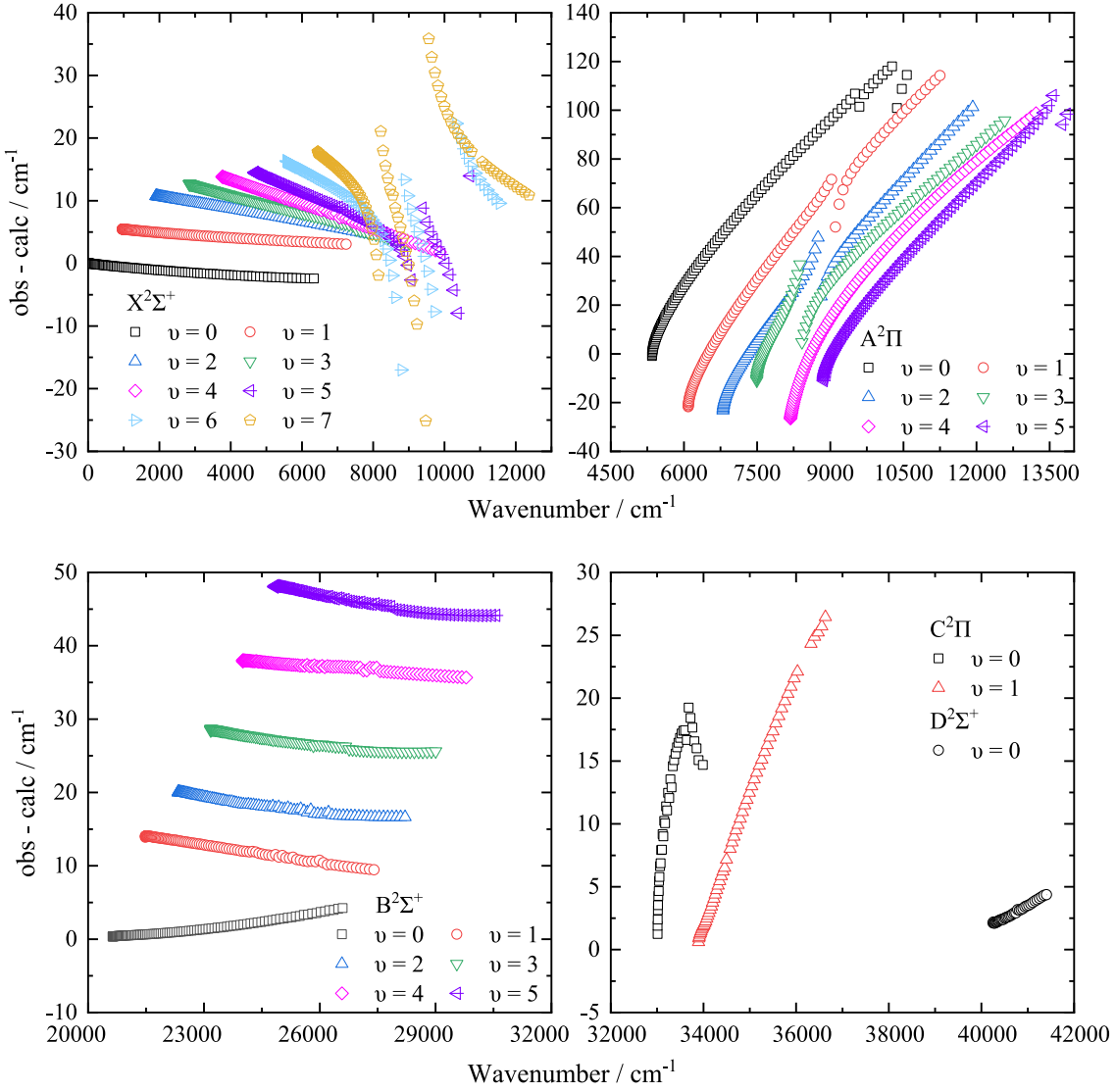

Fig. 2. Residual errors (obs. – calc.) between the empirically derived MARVEL energy levels of AlO ($X^2\Sigma^+$, $A^2\Pi$, $B^2\Sigma^+$, $C^2\Pi$ and $D^2\Sigma^+$) [27] and our calculated values.

where n is the n-th electronic state. $E_{n,\upsilon,l}$ is the energy of the n-th electronic state with quantum numbers, Λ, υ, l. ε_0 refers to the energy of the lowest energy level.

The emission line intensity (erg (smolecule·sr)$^{-1}$) can be given by [46]

$$e(i \to f) = \frac{g_i^{tot} A_{fi} hc\nu_{if}}{4\pi Q(T)} \exp\left(-hcE_i/k_B T\right) \tag{5}$$

By introducing a line profile $f(\nu - \nu_{fi})$, the absorption cross section from a transition $f \leftarrow i$ can be defined as [46]

$$\sigma^{abs}(f \leftarrow i) = I(f \leftarrow i) f\left(\nu - \nu_{fi}\right) \tag{6}$$

The emission cross section can also be expressed by

$$\sigma^{emi}(i \to f) = e(i \to f) f\left(\nu - \nu_{if}\right) \tag{7}$$

3. Results

3.1. Potential energy curves

The ground states of the Al and O atoms are ^2P_u ($3s^2 3p$) and ^3P_g ($2s^2 2p^4$), respectively. The first excited state of the O atom is ^1D_g ($2s^2 2p^4$), whose energy is 15,867.86 cm^{-1} relative to its ground

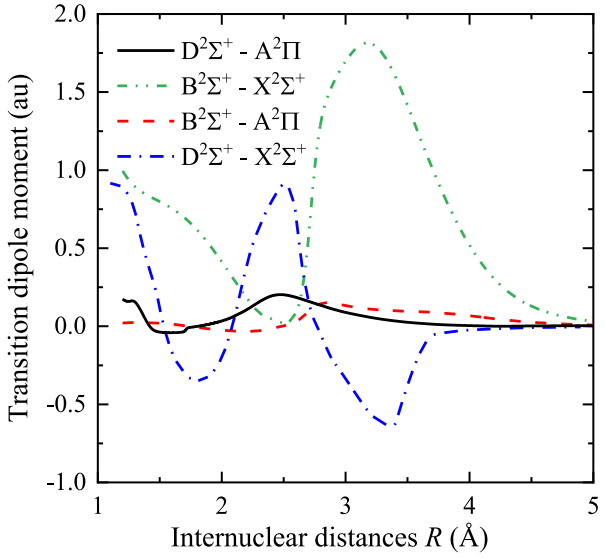

Fig. 3. Transition dipole moments between different electronic states of AlO.

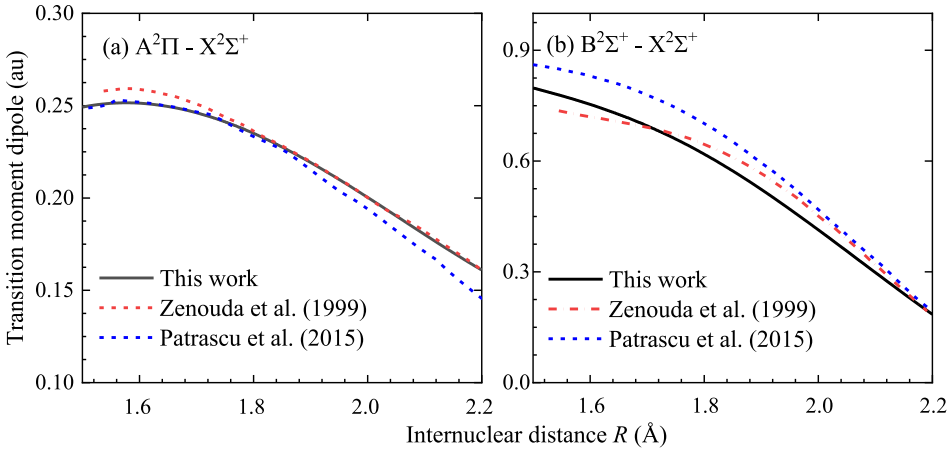

Fig. 4. Comparisons of the transition dipole moments for the $A^2\Pi$ - $X^2\Sigma^+$ and $B^2\Sigma^+$ - $X^2\Sigma^+$ transitions with the theoretical [37,38] values.

Table 1
Dissociation relationships of sixteen Λ-Ω states of AlO.

Separated-atom Atomic States	Molecular states	Dissociation limit (cm^{-1})	
		Experiment [48]	This work
Al ($3s^2 3p\ ^2P_u$) + O ($2s^2 2p^4\ ^3P_g$)	$X^2\Sigma^+$, $A^2\Pi$, $C^2\Pi$, $1^2\Sigma^-$, $1^2\Delta$, $2^2\Sigma^-$, $1^4\Sigma^+$, $1^4\Pi$, $2^4\Pi$, $1^4\Sigma^-$, $1^4\Delta$, $2^4\Sigma^-$	0	0
Al ($3s^2 3p\ ^2P_u$) + O ($2s^2 2p^4\ ^1D_g$)	$B^2\Sigma^+$, $D^2\Sigma^+$, $1'^2\Pi$, $1''^2\Pi$	15,867.86	15,816.24

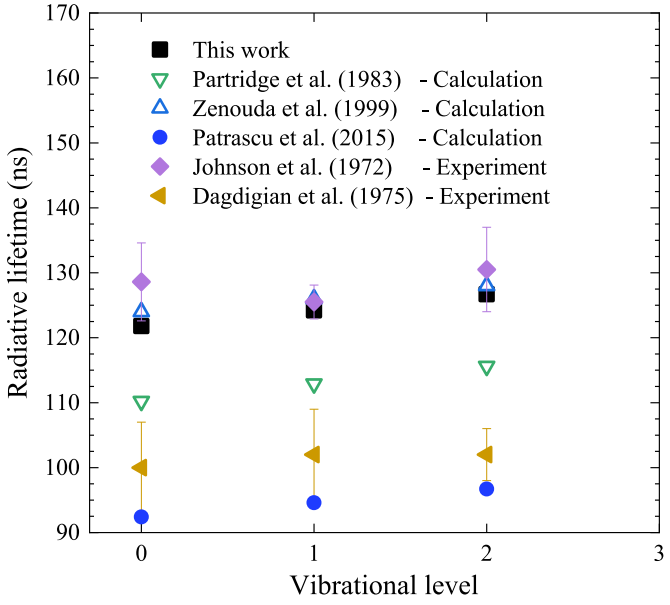

Fig. 5. A comparison of the vibrational radiative lifetimes of the $B^2\Sigma^+$ state with previous theoretical [37,38,52] and experimental values [22,56].

state [48]. Hence, the first and second dissociation limits of the AlO radical are Al ($3s^2 3p\ ^2P_u$) + O ($2s^2 2p^4\ ^3P_g$) and Al ($3s^2 3p\ ^2P_u$) + O ($2s^2 2p^4\ ^1D_g$), respectively. Table 1 shows the molecular states of AlO resulting from the related atomic states. The energy difference between the first and second dissociation limits was calculated to be 15,816.24 cm^{-1}, which is in good agreement with the experimental value of 15,867.86 cm^{-1} [48].

The PECs of sixteen electronic states of AlO are plotted in Fig. 1, where the PECs of the states correlating to the first dissociation limit have been investigated for the collision of the aluminium and oxygen atoms in their electronic ground states [49]. Electronic states including the $B^2\Sigma^+$, $D^2\Sigma^+$, $1'^2\Pi$ and $1''^2\Pi$ states correlating to the second dissociation limit were calculated in this work. A barrier on the PEC of the $B^2\Sigma^+$ state emerges around the internuclear distance R = 2.5 Å to avoid crossing with the PEC of the $D^2\Sigma^+$ state. This was also mentioned by Honjou [50] who investigated the electronic structures of the $X^2\Sigma^+$, $B^2\Sigma^+$, $D^2\Sigma^+$ and $F^2\Sigma^+$ states for AlO.

Spectroscopic constants of the bound $B^2\Sigma^+$and $D^2\Sigma^+$states are calculated and presented in Table 2. Our spectroscopic constants for the $B^2\Sigma^+$ state are in quite good agreement with those determined experimentally, there are slight deviations of about 1.5 cm^{-1} for the harmonic frequency ω_e and of about 230 cm^{-1} for the electronic excitation energy T_e relative to the experiment value [26,51]. For the $D^2\Sigma^+$ state, our equilibrium bond distance is 1.730 Å and the corresponding difference is 0.007 Å with the experiment value [26]. The differences of the ω_e and T_e are about 11 and 455 cm^{-1}, respectively [26]. This may be due to the neglect of the spin-orbit, spin-spin, orbit-orbit couplings and other effects in the calculation of the PECs.

The energy levels are highly sensitive to the values of T_e *and* r_e, thus we modify the calculated PECs by incorporating experimentally derived T_e and r_e values. Compared with the empirically derived MARVEL energy levels, the residual errors are presented in Fig. 2. The residual errors for the $X^2\Sigma^+$, $B^2\Sigma^+$, $C^2\Pi$ and $D^2\Sigma^+$states exhibit an increasing trend with vibrational levels in each electronic state. These errors range between 0 and 50 cm^{-1}. However, the energy level of the $A^2\Pi$ state exhibits larger residual errors, reaching up to about 100 cm^{-1} at higher rotational levels. This can be attributed to the significant deviation between the calculated ω_e and $\omega_e\chi_e$ and the experimental values of the $A^2\Pi$ electronic state.

The uncertainty of the levels is expected to grow with the energy, resulting in a quadratic dependence on J and linear dependence on υ. To estimate these uncertainties, the following approximate expression can be used [53]:

$$unc = a\upsilon + bJ(J+1) + c \tag{8}$$

where a, b and c are electronic state-dependent constant. For the $X^2\Sigma^+$, $A^2\Pi$, $B^2\Sigma^+$, $C^2\Pi$ and $D^2\Sigma^+$ states, uncertainties were estimated based on the progression of residuals from Fig. 2. Overall energy level uncertainties are summarized in Table 3.

Table 2
Spectroscopic constants of the $B^2\Sigma^+$and $D^2\Sigma^+$ states of AlO, along with previous experimental and theoretical ones.

State		T_e/cm^{-1}	R_e/Å	ω_e/cm^{-1}	$\omega_e\chi_e$/cm^{-1}	B_e/cm^{-1}	$10^3\alpha_e$/cm^{-1}
$B^2\Sigma^+$	This work	20,451.02	1.6666	871.74	3.6691	0.634	0.60436
	Exp. [26]	20,688.95	1.6670	870.05	3.52		0.6041
	Exp. [51]	20,685.04		870.37	3.651	0.10	0.6090
	Cal. [28]		1.663	946			
	Cal. [52]	19,628	1.6881	871			
	Cal. [37]	20,192	1.677	869	4.18		
	Cal. [50]	20,625	1.677	846	4.1		
	Cal. [36]	20,534.9	1.6680	875.75	3.9354	9.99	0.6036
$D^2\Sigma^+$	This work	39,811	1.730	808.86	7.33	0.5650	10.48
	Exp. [26]	40,266.7	1.723	819.6	5.8		
	Cal. [28]	40,268	1.727	817.5			
	Cal. [37]	40,685	1.726	833			
	Cal. [50]	40,082	1.728	816	5.8		

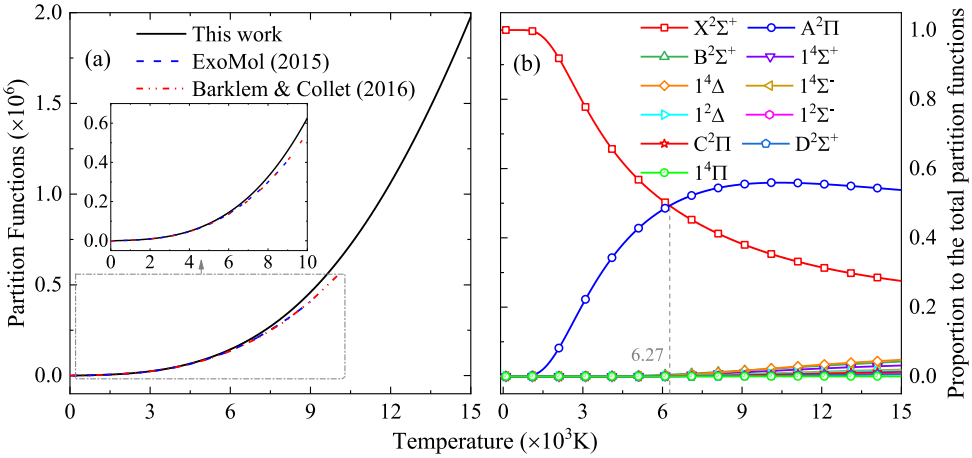

Fig. 6. Curves of (a) the comparison of the partition functions of AlO with those from Barklem and Collet [57] and ExoMol group [38] and (b) the proportion of each electronic state relative to the total partition functions.

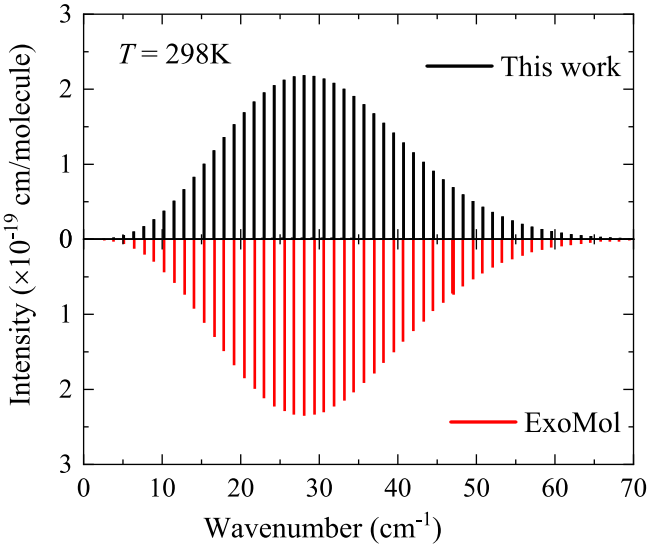

Fig. 7. A comparison of absorption line intensities of the ground state with those in the ExoMol molecular spectroscopy databases.

Table 3
Uncertainty estimates (in cm^{-1}) are applied for the rovibronic energy levels of AlO as a function of state quantum numbers.

State	$\upsilon < 5$	$\upsilon \geq 5$
$X^2\Sigma^+$	$0.0001\,J_X^2 + 0.01J_X + 0.1$, $\upsilon_X = 0$ $-0.0007\,J_X^2 + 0.004\,J_X + 10.7$, $\upsilon_X = 1$ $-0.001\,J_X^2 + 0.003\,J_X + 12.6$, $\upsilon_X = 2$ $-0.001\,J_X^2 + 0.002\,J_X + 13.8$, $\upsilon_X = 3$ $-0.002\,J_X^2 + 0.03\,J_X + 14.1$, $\upsilon_X = 4$	40 - 60
$A^2\Pi$	$0.005\,J_A^2 + 0.8\,J_A - 3.6$, $\upsilon_A = 0$ $0.007\,J_A^2 + 0.6\,J_A - 23.2$, $\upsilon_A = 1,2$ $0.006\,J_A^2 + 0.4\,J_A - 9.0$, $\upsilon_A = 3$ $0.003\,J_A^2 + 1.0\,J_A - 30.7$, $\upsilon_A = 4$	10 - 110
$B^2\Sigma^+$	$0.0006\,J_B^2 - 0.02\,J_B + 0.6$, $\upsilon_B = 0$ $-0.0005\,J_B^2 - 0.0007\,J_B + 14.1$, $\upsilon_B = 1$ $-0.0001\,J_B^2 - 0.03\,J_B + 20.3$, $\upsilon_B = 2$ 20 - 40, $\upsilon_B = 3, 4$	40 - 60
$C^2\Pi$	$-0.01\,J_C^2 + 0.9\,J_C - 0.3$, $\upsilon_C = 0$, $J_C \leq 40$ $0.005\,J_C^2 + 0.2\,J_C + 0.1$, $\upsilon_C = 1$, $J_C \leq 68$ 10 - 40, other υ_C and J_C level	40 - 60
$D^2\Sigma^+$	$0.002\,J_D^2 - 0.02\,J_D + 2.2$, $\upsilon_D = 0,10 \leq J_D \leq 40$ 10 - 30, other υ_D and J_D level	40 - 60
All other states	20 - 40	40 - 60

3.2. Transition dipole moments

Utilizing the icMRCI method, the TDMs for dipole allowed transitions between doublet or quartet states are computed, where those for the $X^2\Sigma^+$ - $A^2\Pi$, $A^2\Pi$ - $1^2\Delta$, $A^2\Pi$ - $2^2\Sigma^-$, $A^2\Pi$ - $1^2\Sigma^-$, $X^2\Sigma^+$ - $1^2\Pi$, $1^2\Pi$ - $1^2\Sigma^-$, $1^2\Pi$ - $A^2\Pi$, $2^4\Pi$ - $1^4\Sigma^+$, $1^4\Pi$ - $1^4\Sigma^-$, $2^4\Pi$ - $1^4\Sigma^-$, $1^4\Pi$ - $1^4\Sigma^+$, $2^4\Pi$ - $1^4\Delta$ and $1^4\Pi$ - $1^4\Delta$ have been investigated in our previous work [49]. The TDMs for the $D^2\Sigma^+$ - $A^2\Pi$, $D^2\Sigma^+$ - $X^2\Sigma^+$, $B^2\Sigma^+$ - $A^2\Pi$ and $B^2\Sigma^+$ - $X^2\Sigma^+$ transitions were calculated in this work, as shown in Fig. 3. The relative phases of the TDMs were selected to be consistent with the phases of the *ab initio* curves produced in our MOLPRO calculations [35]. Comparisons with earlier theoretical and experimental results are displayed in Fig. 4, which indicates that our TDMs

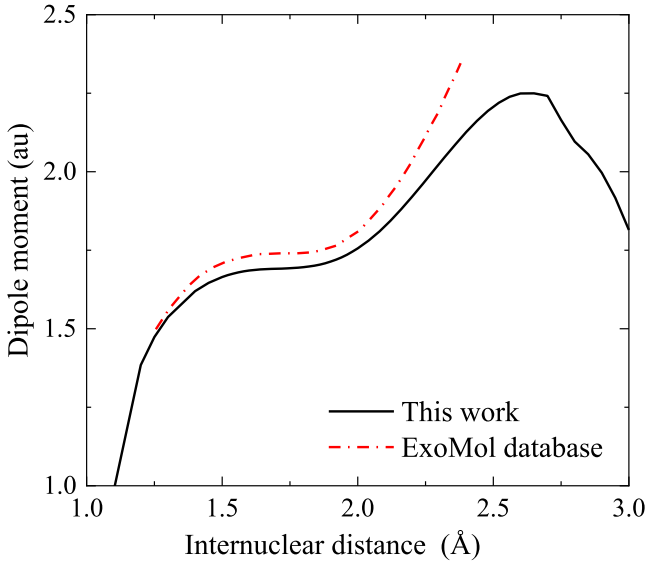

Fig. 8. Dipole moments of the ground state of AlO.

for the $A^2\Pi$ - $X^2\Sigma^+$ and $B^2\Sigma^+$ - $X^2\Sigma^+$ transitions agree well with the previous theoretical results [37,52,54]. It is worth noting that the $B^2\Sigma^+$ state avoids crossing with the higher lying $D^2\Sigma^+$ state near 2.5 Å as it changes its leading electron configuration from $5\sigma^2 6\sigma^1 2\pi^4 7\sigma^2 3\pi^0 8\sigma^0$ to $5\sigma^2 6\sigma^2 2\pi^4 7\sigma^1 3\pi^0 8\sigma^0$, resulting in the large variation in the TDMs of the $B^2\Sigma^+$-$X^2\Sigma^+$ and $B^2\Sigma^+$-$A^2\Pi$ systems near 2.5 Å.

To clearly understand the electronic transitions between different states, electron configurations of these states were calculated. Table 4 lists the leading electron configurations of eleven bound states around their corresponding equilibrium internuclear distances. From these leading electron configurations, we can easily determine which electron undergoes the radiative transition in a certain electronic transition process. Honjou [50] presented the variation in the weights of important electron configurations for the $X^2\Sigma^+$, $B^2\Sigma^+$ and $D^2\Sigma^+$ states with the internuclear distance. Our electron configurations are consistent with those reported by Honjou [50].

3.3. Radiative lifetimes

The blue-green ($B^2\Sigma^+$-$X^2\Sigma^+$) band system of AlO radical has been extensively studied, producing many experimental radiative lifetimes of the $B^2\Sigma^+$ state. The $B^2\Sigma^+$ state can decay to the $X^2\Sigma^+$ and $A^2\Pi$ states, so the $B^2\Sigma^+$ - $X^2\Sigma^+$ and $B^2\Sigma^+$ - $A^2\Pi$ transitions are considered here to calculate the radiative lifetimes of the $B^2\Sigma^+$ state. Einstein coefficients of the $B^2\Sigma^+$ - $X^2\Sigma^+$ and $B^2\Sigma^+$ - $A^2\Pi$ transitions were obtained by solving the nuclear-motion equation over the PECs and TDMs, as implemented in the LEVEL program [55]. The radiative lifetime of each vibrational level of the $B^2\Sigma^+$ state was determined using Eq. (1), where radiative lifetimes of the first three vibrational levels are plotted in Fig. 5 and presented in Table 5, along with previous theoretical and experimental data. Our radiative lifetimes are consistent with those measured by Johnson

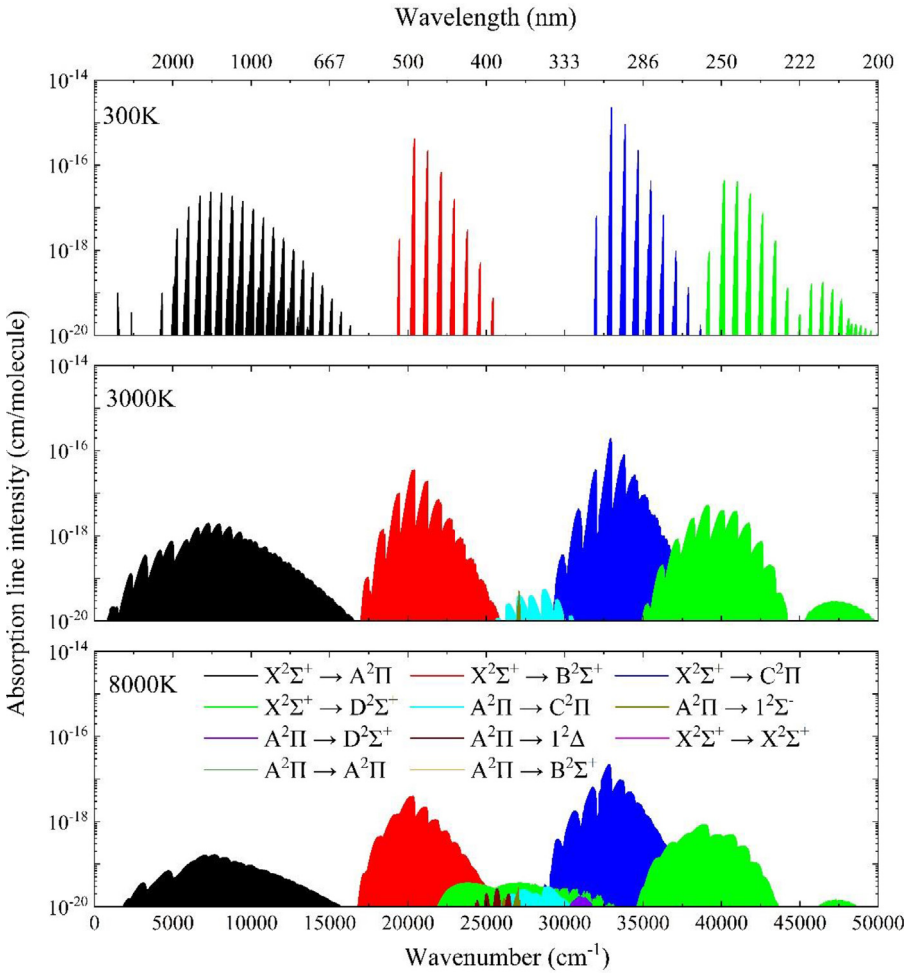

Fig. 9. Absorption line intensities of eleven electronic transition processes of AlO.

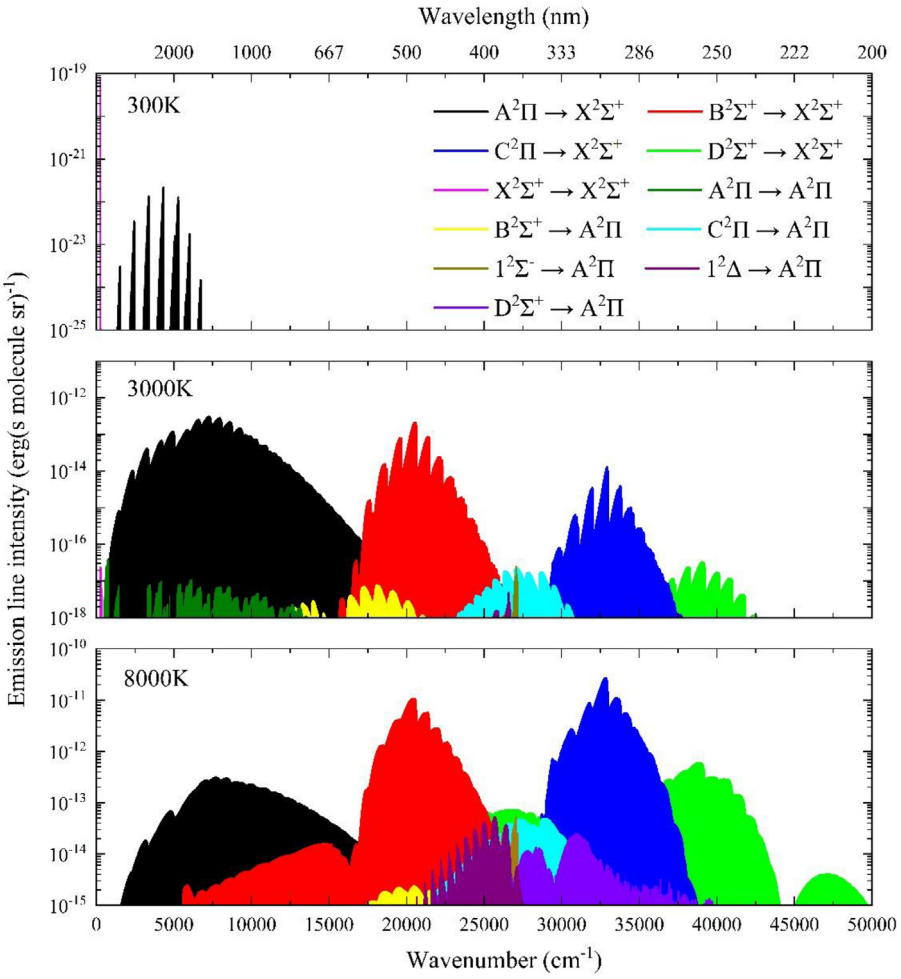

Fig. 10. Emission line intensities of eleven electronic transition processes of AlO.

Table 4
Main electron configurations of electronic states of AlO around their corresponding equilibrium internuclear distances.

Electronic state	Main electron configuration[a]	Electronic state	Main electron configuration[a]
$X^2\Sigma^+$	$5\sigma^2 6\sigma^2 2\pi^4 7\sigma^1 3\pi^0 8\sigma^0$(0.794)	$A^2\Pi$	$5\sigma^2 6\sigma^2 2\pi^3 7\sigma^2 3\pi^0 8\sigma^0$(0.937)
$B^2\Sigma^+$	$5\sigma^2 6\sigma^1 2\pi^4 7\sigma^2 3\pi^0 8\sigma^0$(0.770)	$1^2\Delta$	$5\sigma^2 6\sigma^2 2\pi^3 7\sigma^1 3\pi^1 8\sigma^0$(0.927)
	$5\sigma^2 6\sigma^2 2\pi^4 7\sigma^1 3\pi^0 8\sigma^0$(0.147)		
$1^2\Sigma^-$	$5\sigma^2 6\sigma^2 2\pi^3 7\sigma^1 3\pi^1 8\sigma^0$(0.935)	$C^2\Pi$	$5\sigma^2 6\sigma^2 2\pi^4 7\sigma^0 3\pi^1 8\sigma^0$(0.335)
			$5\sigma^2 6\sigma^1 2\pi^4 7\sigma^1 3\pi^1 8\sigma^0$(0.302)
$D^2\Sigma^+$	$5\sigma^2 6\sigma^2 2\pi^3 7\sigma^1 3\pi^1 8\sigma^0$(0.708)	$1^4\Sigma^+$	$5\sigma^2 6\sigma^2 2\pi^3 7\sigma^1 3\pi^1 8\sigma^0$(0.671)
			$5\sigma^2 6\sigma^2 2\pi^3 7\sigma^0 3\pi^1 8\sigma^1$(0.066)
$1^4\Delta$	$5\sigma^2 6\sigma^2 2\pi^3 7\sigma^1 3\pi^1 8\sigma^0$(0.669)	$1^4\Sigma^-$	$5\sigma^2 6\sigma^2 2\pi^3 7\sigma^1 3\pi^1 8\sigma^0$(0.666)
	$5\sigma^2 6\sigma^2 2\pi^3 7\sigma^0 3\pi^1 8\sigma^1$(0.070)		$5\sigma^2 6\sigma^2 2\pi^3 7\sigma^0 3\pi^1 8\sigma^1$(0.071)
$1^4\Pi$	$5\sigma^2 6\sigma^1 2\pi^4 7\sigma^1 3\pi^1 8\sigma^0$(0.936)		

Notes.
[a] Core configuration is $1\sigma^2 2\sigma^2 3\sigma^2 4\sigma^2 1\pi^4$.

et al. [22] and calculated by Zenouda et al. [37]. However, our radiative lifetimes are longer than those reported by Patrascu et al. [35,38], as our calculated TDMs of the $X^2\Sigma^+ \rightarrow B^2\Sigma^+$ transition are smaller than those used by Patrascu et al. [38], as illustrated in Fig. 4.

Radiative lifetimes of the $A^2\Pi$, $1^2\Delta$, $C^2\Pi$, $1^2\Sigma^-$ and $1^4\Pi$ states were also calculated, as shown in Table 5. The calculated radiative lifetimes of the $A^2\Pi$ states agree with those of Patrascu et al. [38]. The radiative lifetime of the $C^2\Pi$ state at the first vibrational level ($\upsilon' = 0$) has been observed in the experiment and the value is 13 ± 2 ns [23]. Compared with the value calculated by Feng and Zhu, our value is closer to the experimental value and the corresponding difference is only 6.3 ns [39]. For other excited states, only Feng and Zhu [39] have calculated their radiative lifetimes, but their results are not agreement with other theoretical and experimental results. For example, previous theoretical and experimental radiative lifetimes of the $B^2\Sigma^+$ state at the first vibrational level ranged from 100 to 130 ns, but the value calculated by Feng and Zhu was 233 ns [39], and thus their results may be questionable.

3.4. Intensities

Partition functions of AlO versus the temperatures of 10 ~ 15,000 K were calculated using the rovibrational energy levels of eleven electronic states ($X^2\Sigma^+$, $A^2\Pi$, $B^2\Sigma^+$, $1^4\Sigma^+$, $1^4\Delta$, $1^4\Sigma^-$,

Table 5
Vibrational radiative lifetimes of the $A^2\Pi$ state via the $A^2\Pi$ - $X^2\Sigma^+$ transition, of the $B^2\Sigma^+$ state via the $B^2\Sigma^+$ - $X^2\Sigma^+$ and $B^2\Sigma^+$ - $A^2\Pi$ transitions, of the $1^2\Delta$ state via the $1^2\Delta$ - $A^2\Pi$ transition, of the $C^2\Pi$ state via the $C^2\Pi$ - $X^2\Sigma^+$, $C^2\Pi$ - $A^2\Pi$ and $C^2\Pi$ - $B^2\Sigma^+$ transitions, and of the $1^4\Pi$ state via the $1^4\Pi$ - $1^4\Delta$, $1^4\Pi$ - $1^4\Sigma^+$ and $1^4\Pi$ - $1^4\Sigma^-$transitions.

v'		0	1	2	3	4	5	6
$A^2\Pi$[a]	This work	107.4	61.5	41.3	32.7	27.9	23.8	21.0
	Cal. [38]	107.8	65.1	47.8	38.8	37.6	28.0	25.0
	Cal. [39]	162.4	106.4	80.6	65.7	55.9	49.0	43.8
$B^2\Sigma^+$[b]	This work	121.8	124.2	126.7	129.2	131.7	134.2	136.8
	Exp. [22]	128.6 ± 6	125.5 ± 2.6	130.5 ± 6.5				
	Exp. [56]	100 ± 7	102 ± 7	102 ± 7				
	Cal. [38]	92.4	94.6	96.7	99.0	101.2	103.6	106.6
	Cal. [37]	124	126	128				
	Cal. [52]	110.2	112.9	115.6				
	Cal. [39]	233	235	236	238	239	241	242
$1^2\Delta$[a]	This work	90.0	55.6	38.0	27.4	20.3	15.4	11.9
	Cal. [39]	504.8	450.0	364.0	263.3	175.5	113.3	73.3
$C^2\Pi$[b]	This work	19.3	19.5	19.9	20.1	20.4	20.6	21.0
	Exp. [23]	13 ± 2						
	Cal. [39]	51.0	50.8	50.5	50.2	49.8	49.3	48.8
$1^2\Sigma^-$[a]	This work	7.0	6.4	5.9	5.4	4.8	4.4	3.9
$1^4\Pi$[a]	This work	13.7	7.6	5.8	4.4	3.4	2.6	2.0

Notes.
[a] The unit of the radiative lifetime is μs.
[b] The unit of the radiative lifetime is ns.

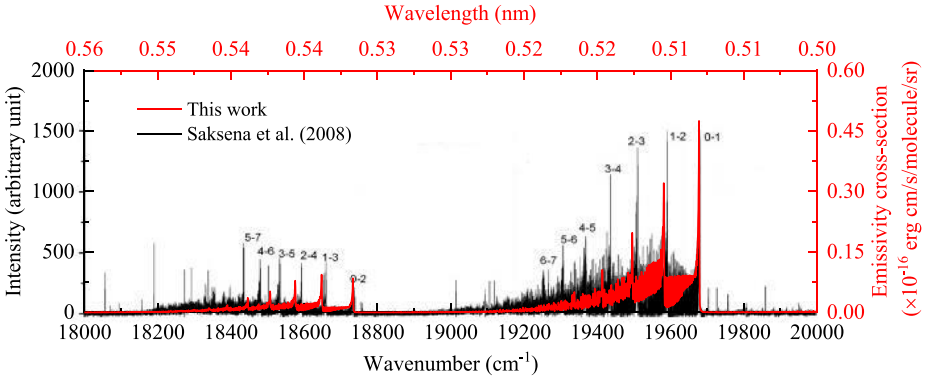

Fig. 11. A comparison of our calculated emission cross sections of the $B^2\Sigma^+ - X^2\Sigma^+$ transition using a Voigt line shape at T = 1700 K and p = 1 atm [51] with the experimental data from Saksena et al. for the wavenumbers of 18,000 ~ 20,000 cm^{-1}.

$1^2\Delta$, $1^2\Sigma^-$, $C^2\Pi$, $D^2\Sigma^+$ and $1^4\Pi$) and displayed in Fig. 6(a). Barklem and Collet [57] calculated the vibrational and rotational energies based on Dunham expansion using the experimental spectroscopic data of the $X^2\Sigma^+$, $A^2\Pi$, $B^2\Sigma^+$, $C^2\Pi$ and $D^2\Sigma^+$ states and then obtained the partition functions of AlO for the temperatures of 0.0001 ~ 10,000 K. We considered more electronic states and thus our partition functions are larger than those given by Barklem and Collet [57] at high temperatures. In addition, the ExoMol group [38] also calculated the partition functions of AlO for the temperatures of 10 ~ 8000 K, but only three electronic states ($X^2\Sigma^+$, $A^2\Pi$ and $B^2\Sigma^+$) are considered. As a result, the partition functions of the ExoMol group are also smaller than our values at high temperatures.

To investigate the contributions of different states to the total partition functions, the proportion of a specific electronic state to the total partition functions can be determined. For example, the proportion of the $B^2\Sigma^+$ state can be computed by

$$w_{B^2\Sigma^+} = \frac{Q_{X^2\Sigma^+ + A^2\Pi + B^2\Sigma^+}(T) - Q_{X^2\Sigma^+ + A^2\Pi}(T)}{Q_{\text{total}}(T)} \quad (9)$$

where $Q_{X^2\Sigma^+ + A^2\Pi + B^2\Sigma^+}(T)$ are the partition functions considering the $X^2\Sigma^+$, $A^2\Pi$ and $B^2\Sigma^+$ states, $Q_{\text{total}}(T)$ are the total partition functions considering eleven electronic states mentioned above. The proportion of each state is plotted in Fig. 6(b), which shows that the AlO molecules mainly exist in the $X^2\Sigma^+$ state at the temperatures of 10 ~ 6270 K and in the $A^2\Pi$ state at the temperatures of 6270 ~ 15,000 K.

Based on Einstein coefficients and partition functions, absorption line intensities can be calculated. Fig. 7 shows a comparison of our calculated rotational spectrum of the $X^2\Sigma^+$ state with that from the ExoMol database [38]. It can be found that the line positions calculated in this work are in good agreement with those in the ExoMol database. However, our line intensities are slightly lower than those given in the ExoMol database. Such difference maybe results from the TDM values used, as shown in Fig. 8.

The absorption and emission line intensities of eleven electronic transitions of AlO were calculated and shown in Fig. 9 and Fig. 10, respectively, where the line intensities of the $X^2\Sigma^+ - A^2\Pi$ and $X^2\Sigma^+ - B^2\Sigma^+$ transitions are strong in the infrared waveband, the $X^2\Sigma^+ - B^2\Sigma^+$, $A^2\Pi - C^2\Pi$, $A^2\Pi - 1^2\Sigma^-$, $A^2\Pi - 1^2\Delta$, $X^2\Sigma^+ - D^2\Sigma^+$ and $A^2\Pi - D^2\Sigma^+$ transitions have strong radiation in the visible waveband, and the $X^2\Sigma^+ - C^2\Pi$ and $X^2\Sigma^+ - D^2\Sigma^+$ transitions work in the ultraviolet waveband.

As the temperature increases, the peak value of the absorption line intensity of each transition decreases gradually. For low temperatures, the ground state mainly absorbs energy to be excited, because the AlO molecules mainly exist in the ground state at temperatures of 10 ~ 6270 K. For example, the $X^2\Sigma^+ \rightarrow A^2\Pi$, $X^2\Sigma^+ \rightarrow B^2\Sigma^+$, $X^2\Sigma^+ \rightarrow C^2\Pi$ and $X^2\Sigma^+ \rightarrow D^2\Sigma^+$ transitions have strong line intensities at 3000 K. As the temperature in-

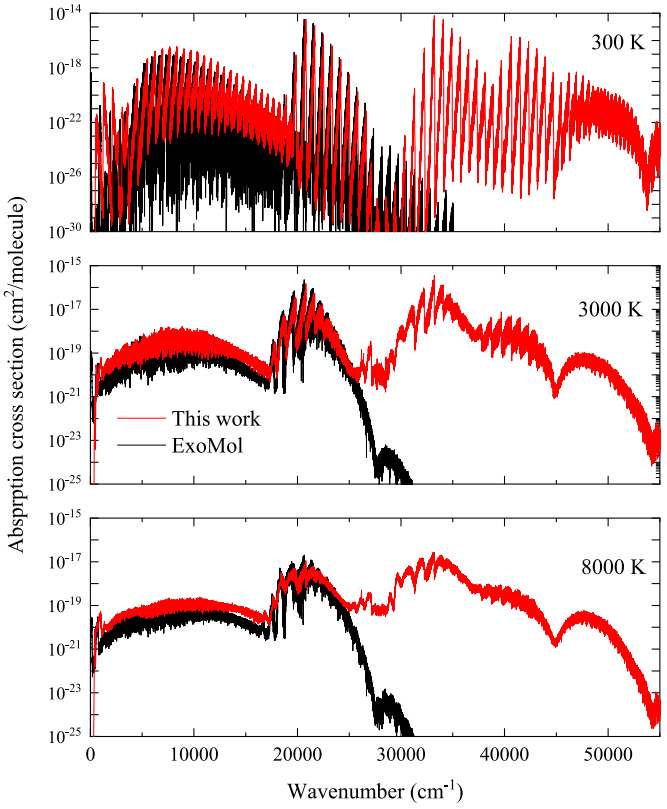

Fig. 12. A comparison of our calculated absorption cross sections at T = 300 K, 3000 K and 8000 K with those from Patrascu et al. [35,38].

creases, the transition from the $A^2\Pi$ state gradually works at 8000 K, since the AlO molecules mainly exist in the $A^2\Pi$ state. However, their absorption line intensities are weak at 8000 K because of the small TDMs of the $A^2\Pi \rightarrow C^2\Pi$, $A^2\Pi \rightarrow 1^2\Sigma^-$, $A^2\Pi \rightarrow 1^2\Delta$ and $A^2\Pi \rightarrow D^2\Sigma^+$ transitions near the equilibrium internuclear distances.

Fig. 10 shows the emission line intensities of eleven electronic transitions at 300 K, 3000 K and 8000 K. For low temperatures, the transition processes from the $A^2\Pi$, $B^2\Sigma^+$ and $C^2\Pi$ states to the ground state play a key role. As the temperature increases, the emission line intensity increases gradually, and the de-excitation of the $D^2\Sigma^+$ becomes an important process.

3.5. Cross sections

The blue-green ($B^2\Sigma^+ - X^2\Sigma^+$) band of AlO is widely observed in the experiments. Saksena et al. [51] observed the spectrum at high vibrational levels ($\upsilon' - \upsilon''$ = 3 − 2, 4 − 3, 2 − 3, 3 − 4, 4 − 5, 5 − 6 and 6 − 7) at the rotational temperature of about 1700 K for the first time. We reproduce the spectrum of AlO at 1700 K and 1 atm using a Voigt line shape, as shown in Fig. 11. Our calculated positions and intensities of the spectral lines are basically consistent with those observed in the experiment for the transitions between the low vibrational levels. However, with the increasing vibrational levels, there are some differences between our calculated results and the experimental data, which may result from the neglect of the spin-orbit, spin-spin, orbit-orbit, spin-other-orbit couplings and other effects in our calculation of the PECs [58]. Also, we only considered the spectrum of $^{27}Al^{16}O$ in the local thermal equilibrium (LTE). The spectra of other isotopes in the LTE or non-LTE may also contribute. In addition, the pressure of 1 atm was used in this work, which was not mentioned in the experiment.

Absorption cross sections of AlO at T = 300 K, 3000 K and 8000 K were calculated to compare with those reported by Patrascu et al. [35,38], as shown in Fig. 12. The results indicate that the absorption cross sections for the $X^2\Sigma^+ \rightarrow A^2\Pi$ transition are generally larger than those reported by Patrascu et al. for wavenumbers ranging from 600 cm^{-1} to 18,000 cm^{-1}, while the calculated absorption cross sections for the $X^2\Sigma^+ \rightarrow B^2\Sigma^+$ transition are generally smaller for wavenumbers ranging from 18,000 cm^{-1} to 24,000 cm^{-1}. These differences are expected, since the TDMs we employed for the $X^2\Sigma^+ \rightarrow A^2\Pi$ and $X^2\Sigma^+ \rightarrow B^2\Sigma^+$ transitions are distinct from those used by Patrascu et al. [38], as illustrated in Fig. 4. Furthermore, the transition wavenumbers we have obtained also differ from those reported by Patrascu et al. [35,38], which can be attributed to the presence of residual errors.

Absorption cross sections of AlO at different temperatures were calculated and presented in Fig. 13. With the temperatures increasing, the absorption cross sections become gradually flat, and the difference with temperature is notable around 30,000 cm^{-1}. Fig. 14 shows the contribution of each transition to the total absorption cross section at 3000 K. The $X^2\Sigma^+ \rightarrow A^2\Pi$, $X^2\Sigma^+ \rightarrow B^2\Sigma^+$, $X^2\Sigma^+ \rightarrow C^2\Pi$ and $X^2\Sigma^+ \rightarrow D^2\Sigma^+$ transitions play dominant roles at different wavebands, where the $X^2\Sigma^+ \rightarrow A^2\Pi$ transition dominates in the infrared waveband. The $X^2\Sigma^+ \rightarrow B^2\Sigma^+$ transition plays a dominant role in the visible waveband, which is consistent with the blue-green band observed in the experiments [18–22]. As the wavenumber increases, the $X^2\Sigma^+ \rightarrow C^2\Pi$

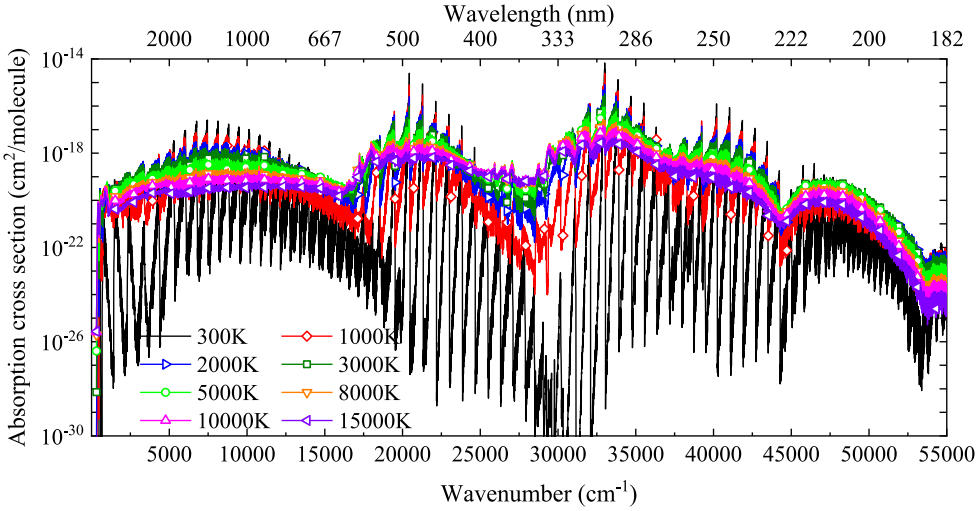

Fig. 13. Temperature dependence of the absorption cross sections of AlO using a Voigt line shape.

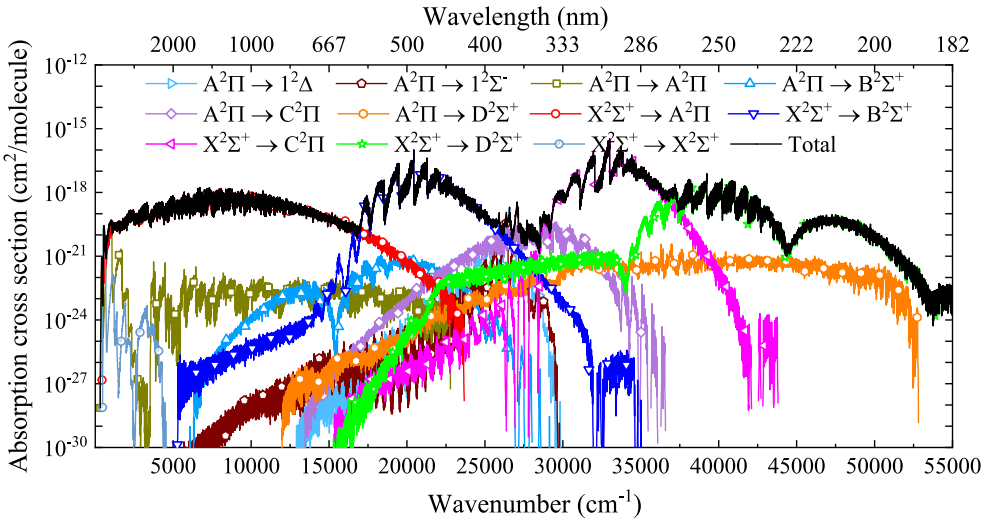

Fig. 14. The contribution of each transition to the total absorption cross section at 3000 K using a Voigt line shape.

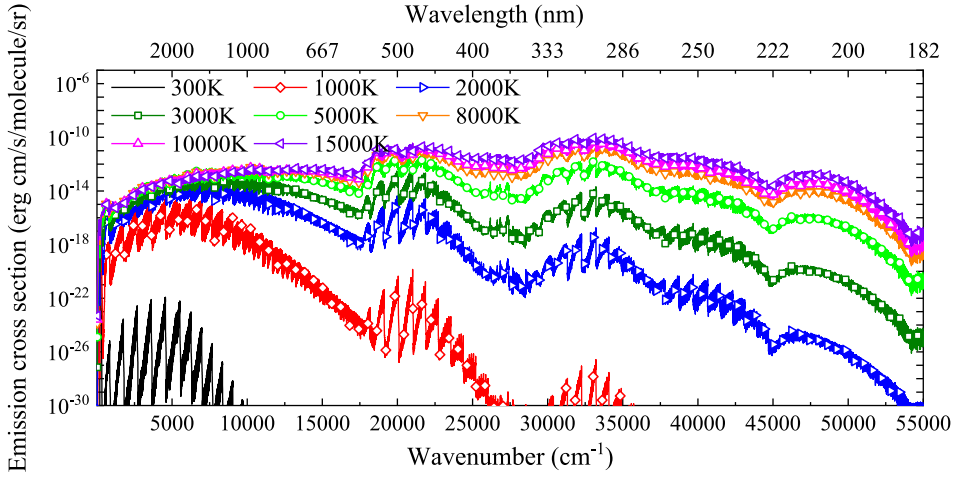

Fig. 15. Temperature dependence of the emission cross sections of AlO using a Voigt line shape.

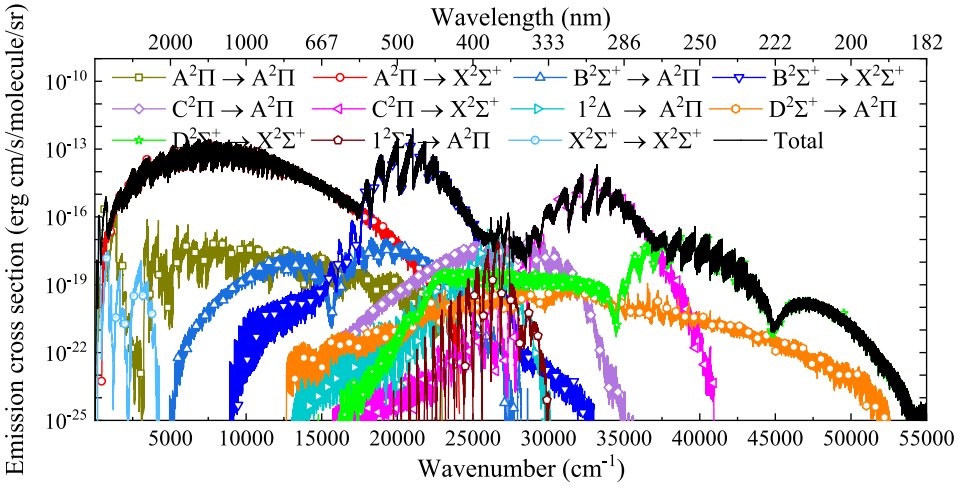

Fig. 16. The contribution of each transition to the total emission cross section at 3000 K using a Voigt line shape.

and $X^2\Sigma^+ \rightarrow D^2\Sigma^+$ transitions dominate in the ultraviolet waveband.

Fig. 15 shows the emission cross sections of AlO at different temperatures. For low temperatures, the emission cross sections are large in the infrared waveband, and they gradually decrease with the increasing wavenumbers. As the temperature increases, the emission cross sections gradually increase at different wavebands, but the increase gradually slows down above 8000 K. Fig. 16 shows the contribution of each transition to the total emission cross sections at 3000 K. The main emission processes are similar to the main absorption processes at a specific waveband.

4. Conclusions

In this work, *ab initio* spectra of AlO have been presented at the temperatures of 300 ~ 15,000 K. PECs of four states ($B^2\Sigma^+$, $D^2\Sigma^+$, $1'^2\Pi$ and $1''^2\Pi$) and TDMs of four transitions ($X^2\Sigma^+ \rightarrow A^2\Pi$, $X^2\Sigma^+ \rightarrow B^2\Sigma^+$, $X^2\Sigma^+ \rightarrow C^2\Pi$ and $X^2\Sigma^+ \rightarrow D^2\Sigma^+$) were calculated at the icMRCI/aug-cc-pwCV5Z-DK level of theory to complement our previous *ab initio* data, and the PECs were modified by incorporating experimentally derived T_e and r_e values. The obtained PECs and TDMs were then introduced the nuclear-motion Schrödinger equation to obtain partition functions, Einstein coefficients, radiative lifetimes, line intensities and spectra of AlO. The partition functions reveal AlO molecules mainly exist in the $X^2\Sigma^+$ state for the temperatures of 10–6270 K and in the $A^2\Pi$ state for the temperatures of 6270–15,000 K. Compared with the previous theoretical results, our calculated radiative lifetimes are closer to the experimental data.

In the calculations of line intensities and spectra, eleven transitions were considered. Our calculated absorption line intensities for the ground state and the absorption cross sections of the $X^2\Sigma^+ \rightarrow A^2\Pi$ and $X^2\Sigma^+ \rightarrow B^2\Sigma^+$ transitions are close to those in the ExoMol database. This indicates our calculated data in the ultraviolet waveband is dependable and may be used for the planetary exploration and radiation field calculation.

Data availability statement

All data are available in this article and in its online supplementary material. The supplementary material includes the PECs of fourteen electronic states, TDMs for four transitions, Einstein coefficients of the $X^2\Sigma^+ \rightarrow A^2\Pi$, $X^2\Sigma^+ \rightarrow B^2\Sigma^+$, $X^2\Sigma^+ \rightarrow C^2\Pi$ and $X^2\Sigma^+ \rightarrow D^2\Sigma^+$ transitions, and absorption and emission cross sections at T = 300 K, 1000 K, 2000 K, 3000 K, 5000 K, 8000 K, 10,000 K, 15,000 K and p = 1atm with a resolution of 1 cm^{-1}.

Declaration of Competing Interest

The authors declare that they have no known competing financial interests or personal relationships that could have appeared to influence the work reported in this paper.

CRediT authorship contribution statement

Tianrui Bai: Software, Investigation, Conceptualization, Methodology, Writing – original draft, Writing – review & editing. **Zhi Qin:** Investigation, Methodology, Writing – review & editing. **Linhua Liu:** Supervision, Funding acquisition, Conceptualization, Writing – review & editing.

Acknowledgments

The support provided by The National Natural Science Foundation of China (52106098) is greatly acknowledged. Qin Zhi also acknowledges the support provided by The Natural Science Foundation of Shandong Province (ZR2021QE021), Postdoctoral Innovation Project of Shandong Province, and Postdoctoral Applied Research Project of Qingdao City.

Supplementary materials

Supplementary material associated with this article can be found, in the online version, at doi:10.1016/j.jqsrt.2023.108587.

References

[1] Kamiński T, Schmidt M, Menten K. Aluminium oxide in the optical spectrum of VY Canis Majoris [J]. Astron Astrophys 2013;549:A6.
[2] Banerjee D, Varricatt W, Mathew B, Launila O, Ashok N. The A-X infrared bands of aluminum oxide in stars: search and new detections [J]. Astrophys J Lett 2012;753:L20.
[3] Banerjee DPK, Varricatt PW, Ashok NM, Launila O. Remarkable changes in the near-infrared spectrum of the nova-like variable V4332 Sgr [J]. Astrophys J 2003;598:L31.
[4] Sriramachandran P, Viswanathan B, Shanmugavel R. Occurrence of AlO molecular lines in sunspot umbral spectra [J]. Sol Phys 2013;286:315–26.
[5] De Beck E, Decin L, Ramstedt S, Olofsson H, Menten K, Patel N, et al. Search for aluminium monoxide in the winds of oxygen-rich AGB stars [J]. Astron Astrophys 2017;598:A53.
[6] Merrill PW, Deutsch AJ, Keenan PC. Absorption Spectra of M-type mira variables [J]. Astrophys J 1962;136:21–33.
[7] Keenan PC, Deutsch AJ, Garrison RF. The anomalous behavior of aluminum oxide bands in mira variables [J]. Food Addit Contam 1969;11:605–614.
[8] Barnbaum C, Omont A, Morris M. The unusual circumstellar environment of the evolved star, U equulei [J]. Astron Astrophys 1996;310:259–70.
[9] Tylenda R, Crause LA, Górny SK, Schmidt MR. V4332 sagittarii revisited [J]. Astron Astrophys 2005;439:651–61.
[10] Tenenbaum ED, Ziurys LM. Millimeter detection of AlO ($X^2\Sigma^+$): metal oxide chemistry in the envelope of VY canis majoris [J]. Astrophys J 2009;694:L59.
[11] Sriramachandran P, Shanmugavel R. Occurrence of AlO molecular lines in sunspot umbral spectra [J]. Sol Phys 2013;286:315–26.
[12] Kraus D, Saykally RJ, Bondybey VE. Cavity-ringdown spectroscopy studies of the $B^2\Sigma^+ \leftarrow X^2\Sigma^+$ rsystem of AlO [J]. ChemPhysChem 2002;3:364–366.
[13] Rosenberg NW, Golomb D, Jr EFA. Resonance radiation of AlO from trimethyl aluminum released into the upper atmosphere [J]. J Geophys Res 1964;69:1451–4.
[14] Johnson ER. Twilight resonance radiation of AlO in the upper atmosphere [J]. J Geophys Res 1965;70:1275–7.
[15] Gole JL, Kolb CE. On the upper atmospheric chemiluminescent emission observed upon release of aluminum vapor and its compounds [J]. J Geophys Res Space Phys 1981;86:9125–36.
[16] Pomeroy WC. The quantum analysis of the band spectrum of aluminum oxide (λ5200-λ4650) [J]. Phys Rev 1927;29:59–78.
[17] Launila O, Jonsson J. Spectroscopy of AlO: rotational analysis of the $A^2\Pi i$ – $X^2\Sigma^+$ transition in the 2-μm region [J]. J Mol Spectrosc 1994;168:1–38.
[18] Rosenwaks S, Steele R, Broida H. Chemiluminescence of AlO [J]. J Chem Phys 1975;63:1963–5.
[19] Hebert G, Tyte D. Intensity measurements on the $A^2\Sigma$ – $X^2\Sigma$ system of aluminium oxide [J]. In: Proceedings of the physical society (1958-1967), 83; 1964. p. 629–34.
[20] Stojadinović S, Perić M, Petković M, Vasilić R, Kasalica B, Belča I, et al. Luminescence of the $B^2\Sigma^+$ – $X^2\Sigma^+$ band system of AlO during plasma electrolytic oxidation of aluminum [J]. Electrochim. Acta 2011;56:10122–10129.
[21] Bai X, Steimle TC. The stark effect, zeeman effect, and transition dipole moments for the $B^2\Sigma^+$ – $X^2\Sigma^+$ band of aluminum monoxide, AlO [J]. Astrophys J 2020;889:147.
[22] Johnson SE, Capelle G, Broida HP. Laser excited fluorescence and radiative lifetimes of AlO ($B^2\Sigma^+$ – $X^2\Sigma^+$) [J]. J Chem Phys 1972;56:663–5.
[23] Towle JP, James AM, Bourne OL, Simard B. The $C^2\Pi$ – $X^2\Sigma^+(0, 0)$ band in AlO [J]. J Mol Spectrosc 1994;163:300–8.
[24] Singh M, Saksena M. A new electronic transition $C^2\Pi r$ – $A^2\Pi i$ of AlO [J]. Can J Phys 1982;60:1730–42.
[25] Tyte D. Red ($B^2\Pi$–$A^2\Sigma$) band system of aluminium monoxide [J]. Nature 1964;202:383–4.
[26] Huber KP, Herzberg G. Molecular spectra and molecular structure: iv constants of diatomic molecules. New York: Elsevier; 1979.
[27] Bowesman CA, Shuai M, Yurchenko SN, Tennyson J. A high-resolution line list for AlO [J]. Mon Not R Astron Soc 2021;508:3181–93.
[28] Schamps J. The energy spectrum of aluminium monoxide [J]. Chem Phys 1973;2:352–66.
[29] Yoshimine M, McLean AD, Liu B. Band strengths for the electric dipole transitions from *ab initio* computation: liO($X^2\Pi$ - $X^2\Pi$), ($A^2\Sigma^+$ - $A^2\Sigma^+$), ($X^2\Pi$ - $A^2\Sigma^+$); AlO($X^2\Sigma^+$ - $X^2\Sigma^+$), ($A^2\Pi$ - $A^2\Pi$), ($X^2\Sigma^+$ - $A^2\Pi$), ($B^2\Sigma^+$ - $B^2\Sigma^+$), ($X^2\Sigma^+$ - $B^2\Sigma^+$) [J]. J Chem Phys 1973;58:4412–29.
[30] Das G, Janis T, Wahl AC. Ground and excited states of the diatoms CN and AlO [J]. J Chem Phys 1974;61:1274–9.

[31] Lengsfield BH, Liu B. *Ab initio* dipole moment functions for the $X^2\Sigma^+$ and $B^2\Sigma^+$ states of AlO [J]. J Chem Phys 1982;77:6083–9.
[32] Kovba VM, Topol IA. Calculations on the electronic structure and spectra of the AlO, GaO and InO molecules by the $X\alpha$ - SW method [J]. J Mol Struct Theochem 1986;137:65–79.
[33] Márquez A, Capitán MJ, Odriozola JA, Sanz JF. Spectroscopic properties and potential energy curves of some low-lying electronic states of AlO, AlO^+, LaO, and LaO^+: an ab initio CASSCF study [J]. Int J Quantum Chem 1994;52:1329–1338.
[34] Honjou N. *Ab initio* study of band strengths for the $F^2\Sigma^+$ – A^2 Π electronic transition of AlO [J]. Comput Theor Chem 2011;978:138–42.
[35] Patrascu A, Hill C, Tennyson J, Yurchenko S. Study of the electronic and rovibronic structure of the $X^2\Sigma^+$, $A^2\Pi$, and $B^2\Sigma^+$ states of AlO [J]. J Chem Phys 2014;141:144312.
[36] Liu H, Shi D, Sun J, Zhu Z. Accurate *ab initio* study on the $A^2\Pi$, $1^4\Sigma^+$, $1^4\Pi$, $2^4\Pi$ and $1^6\Sigma^+$ electronic states of AlO radical including spin-orbit coupling [J]. Spectrochim Acta A Mol Biomol Spectrosc 2013;101:400–9.
[37] Zenouda C, Blottiau P, Chambaud G, Rosmus P. Theoretical study of the electronic states of AlO and AlO^- [J]. J Mol Struct (Theochem) 1999;458:61–72.
[38] Patrascu AT, Yurchenko SN, Tennyson J. ExoMol molecular line lists - IX. The spectrum of AlO [J]. Mon Not R Astron Soc 2015;449:3613–19.
[39] Feng Y, Zhu Z. Rotationless radiative lifetimes and transition probabilities of the seven lowest-lying doublet states of the AlO radical [J]. J Quant Spectrosc Radiat Transf 2019;231:37–48.
[40] Werner HJ, Knowles PJ. An efficient internally contracted multiconfiguration-reference configuration interaction method [J]. J Chem Phys 1988;89:5803–14.
[41] Woon DE, Dunning TH Jr.. Gaussian basis sets for use in correlated molecular calculations. V. core-valence basis sets for boron through neon [J]. J Chem Phys 1995;103:4572–85.
[42] De Jong WA, Harrison RJ, Dixon DA. Parallel Douglas-Kroll energy and gradients in NWChem: estimating scalar relativistic effects using Douglas-Kroll contracted basis sets [J]. J Chem Phys 2001;114:48–53.
[43] Balabanov NB, Peterson KA. Systematically convergent basis sets for transition metals. I. All-electron correlation consistent basis sets for the 3*d* elements *Sc*–Zn [J]. J Chem Phys 2005;123:064107.
[44] Werner HJ, Knowles P, Lindh R, Manby F, Schütz M, Celani P, et al. Molpro, version 2015.1, a package of *ab initio* programs. UK: Cardiff; 2015.
[45] Qin Z, Zhao JM, Liu LH. Radiative transition probabilities for the main diatomic electronic systems of N2, $N2^+$, NO, O2, CO, CO^+, CN, C2 and H2 produced in plasma of atmospheric entry [J]. J Quant Spectrosc Radiat Transf 2017;202:286–301.
[46] Yurchenko SN, Al-Refaie AF, Tennyson J. ExoCross: a general program for generating spectra from molecular line lists [J]. Astron Astrophys 2018;614:A131.
[47] Bai T, Qin Z, Liu L. Thermodynamic and radiative properties of TiO in local thermal equilibrium and non-equilibrium conditions [J]. Mol Phys 2021;119:e1953174.
[48] NIST. 2022.
[49] Bai T, Qin Z, Liu L. Rate coefficients of the aluminium monoxide formation by radiative association [J]. Mon Not R Astron Soc 2022;510:1649–56.
[50] Honjou N. *Ab initio* study of the molecular vibrations and electronic structure of the X, B, D and $F^2\Sigma^+$ states of AlO [J]. J Mol Struct Theochem 2010;939:59–64.
[51] Saksena MD, Deo MN, Sunanda K, Behere SH, Londhe CT. Fourier transform spectral study of $B^2\Sigma^+$ – $X^2\Sigma^+$ system of AlO [J]. J Mol Spectrosc 2008;247:47–56.
[52] Partridge H, Langhoff SR, Lengsfield IIIB, Liu B. Theoretical study of the AlO blue-green ($B^2\Sigma^+$ – $X^2\Sigma^+$) band system [J]. J Quant Spectrosc Radiat Transf 1983;30:449–62.
[53] Semenov M, Clark N, Yurchenko SN, Kim GS, Tennyson J. ExoMol line lists–XLVI. Empirical rovibronic spectra of silicon mononitrate (SiN) covering the six lowest electronic states and four isotopologues [J]. Mon Not R Astron Soc 2022;516:1158–69.
[54] Sato N, Ito H, Kuchitsu K. Electronic transition moment of the AlO($B^2\Sigma^+$ - $X^2\Sigma^+$) emission. Analysis of the R dependence of the $Al^{2+}O^{2-}$ character in the $X^2\Sigma^+$ state [J]. Chem Phys Lett 1995;240:10–16.
[55] le Roy RJ. LEVEL: a computer program for solving the radial Schrödinger equation for bound and quasibound levels [J]. J Quant Spectrosc Radiat Transf 2017;186:167–78.
[56] Dagdigian PJ, Cruse HW, Zare RN. Laser fluorescence study of AlO formed in the reaction Al + O2: product state distribution, dissociation energy, and radiative lifetime [J]. J Chem Phys 1975;62:1824–33.
[57] Barklem PS, Collet R. Partition functions and equilibrium constants for diatomic molecules and atoms of astrophysical interest [J]. Astron Astrophys 2016;588:A96.
[58] John M. Brown, Carrington A. United Kingdom: Cambridge University Press; 2003.